

Astrometry and Relativity

COSTANTINO SIGISMONDI⁽¹⁾

⁽¹⁾ *ICRA, International Center for Relativistic Astrophysics, and University of Rome La Sapienza, Piazzale Aldo Moro 5 00185 Roma, Italy.*

Summary. — General relativistic effects in astrophysical systems have been detected thanks to accurate astrometric measurements. We outline some keystones of astrometry such as stellar aberration (argument development during the years 1727-1872); Mercury's perihelion precession (1845-1916); solar disk oblateness (1966-2001); relativistic light deflection (1916-1919); lunar geodetic precession (1916-1988); Lense-Thirring and Pugh-Schiff precessions (1917-1959), finally presenting the issue of the quest for a guide star for GP-B satellite (1974-2004) as application of all previous topics.

PACS 95.30.S – Relativistic Effects.

PACS 95.10.Jk – Astrometry.

PACS 98.62.Tc – Astrometry.

1. – Stellar aberration

It is a relativistic effect, discovered in 1727 and well explained in a Galilean context. James Bradley discovered it looking for stellar parallaxes. He found that all the stars during a year describe an ellipse with semi-major axis of 20 arcseconds. Galilean explanation is straightforward looking at figure 1: when the Earth is in conjunction with the Sun with respect to a point of view external to the Earth's orbit, the Star appears to be in quadrature with the direction in space drawn by this external point and the Earth. It occurs because of the Galilean composition of velocities.

Regardless of the moduli of the vectorial sums, the directions of the vectors are in agreement with the provenance of starlight. James Bradley in 1727 was looking for stars' parallaxes with respect to background stars (it was actually a Galileo's idea, strongly supported by Kepler, in order to prove the Copernican theory of an orbiting Earth). He expected to see, when the Earth was in quadrature with respect to a given point of the orbit like γ point (i.e. a given direction of space), the star in quadrature with respect to its position with Earth at γ point on the opposite side: a phenomenon which remained unobserved until 1838 (W. Bessel on 61 *Cyg* with the Heliometer of Fraunhofer, see figures 3 and 4) because of the smallness of the effect (< 1 arcsecond).

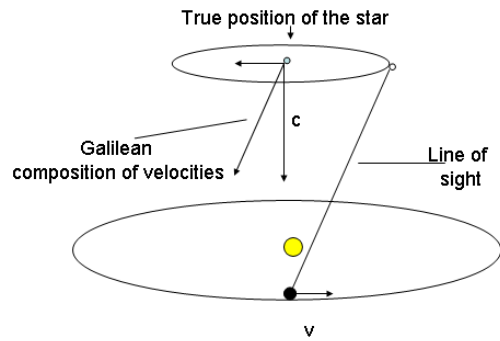


Fig. 1. – Galilean composition of velocities in stellar aberration. The star is near the pole of the Ecliptic in order to magnify the effect.

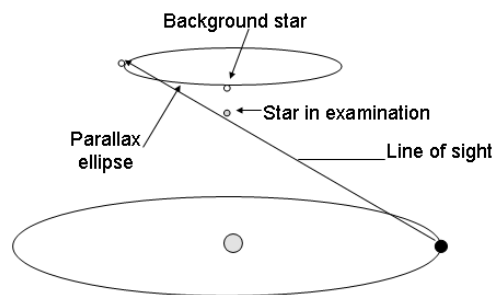


Fig. 2. – Parallax ellipse. The phase of parallax displacement is to be compared with figure 1 of Galilean composition of velocities, their phases are separated of $\pi/2$.

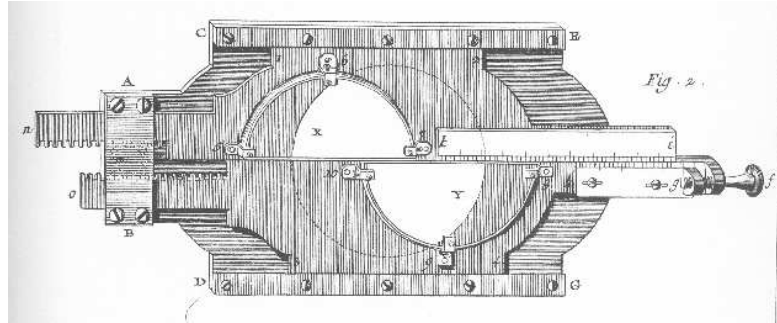


Fig. 3. – Heliumeter. Scheme of the objective lens. Lens is splitted in two halves, which can be moved with a micrometer. They produce two equal images splitted by a quantity depending on the displacement of the two half lenses. The comparison of the position of the star under examination with background stars is made shifting it near them with the micrometer.

Aberration ellipse depends on the ecliptical coordinates of the star: the semi-major axis is $a = v/c = 20$ arcsecs, where v is the orbital velocity of the Earth. The semi-minor axis is approximately $b = v/c \cdot \sin(\beta)$, with β ecliptical latitude of the star. The maximum displacement due to aberration occurs 3 months before the expected parallax effect with respect to background stars.

In the Galilean treatment

$$\tan(\theta - \theta') = v \cdot \sin(\theta) / (c + v \cdot \sin(\theta))$$

or expanding in Taylor series

$$\theta' = \theta - v/c \cdot (\sin(\theta) - 1/2 v/c \cdot \sin(2\theta) + \dots)$$

While in relativistic treatment

$$\tan(\theta') = \tan(\theta) / (1 + v \cdot \sec(\theta) / c) \cdot (1 - v^2/c^2)^{1/2}$$

Phase and group velocity are the same in all inertial frames (for Galilean transformations there is no aberration in phase velocity because the angle of wavefront is an invariant). There came out a question: since stellar light passes through Earth's atmosphere with refraction index n : which velocity is to be used, c or c/n ? In 1872 Airy measured aberration with a telescope filled by water and published the results in the *Proceedings of the Royal Society of London*: the conclusion was that c is to be used for aberration and the atmosphere is solidal with Earth [1, 2].

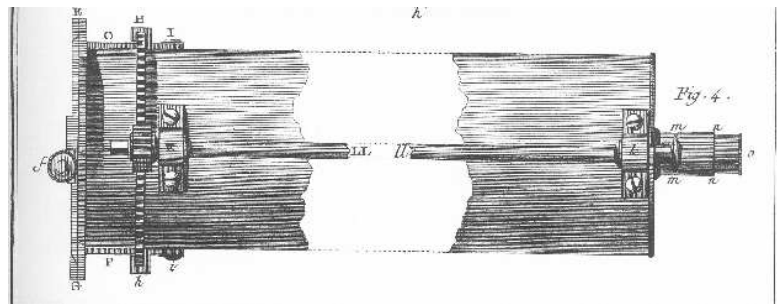


Fig. 4. – Apparatus in order to keep stable the focal length of the telescope with the Heliumeter.

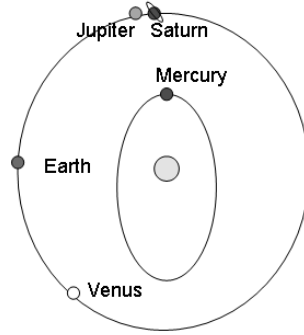


Fig. 5. – Planetary angular displacements after one orbit of Mercury. In this figure all planets start from uppermost position, moving counterclockwise.

2. – Mercury’s perihelion advancement

First attempts were addressed to explain this advancement with Newtonian planetary perturbations. Let us consider as an exemple what happens after a Mercury’s orbit which lasts $\sim 1/4$ year.

The net perturbation of Earth after one orbit of Mercury is $F_{\oplus}/F_{\odot} \sim (m_{\oplus}/m_{\odot}) \cdot (r_{Mercury}/r_{\oplus})^2 \sim 1/200000$ corresponding to a perturbation of 1 arcsec per orbit (~ 200000 arcsecs), i.e. 400 arcsec per century (400 orbits of Mercury per century). But in the case of Earth’s Newtonian perturbations, after 4 Mercury’s orbits, the net balance of Earth’s perturbations almost cancels because of the stability of resonance.

Resonances with all planets are not all exact and a net perturbation arises. Its order of magnitude results the same of Earth’s contribution after one orbit, i.e. ~ 400 arcsecs per century. According to Le Verrier [6] and Newcomb’s [7, 8] observations (1859-1882) all planetary perturbations yield an observed advancement of the perihelion of Mercury’s orbit of 574.10 ± 0.41 arcsec per century. 42.56 ± 0.5 of them remain unexplained by Newtonian theory of gravitation. The reference frame for this advancement is also in motion due to the equinox (lunisolar) precession (discovered by Ipparchus ~ 150 b.C.) of 50 arcsec per year i.e. 5000 arcsec/cy: it is a motion of the Earth’s axis i.e. the celestial pole with respect to the ecliptic pole.

With this motion of the reference frame we include also Nutation, due to the Moon’s influence, another serendipitous discovery (during years 1727-1745) of J. Bradley on γ Draconis whose declination oscillated of ± 18 arcsecs over 18.6 years of observations.

To explain the remaining 42.56 ± 0.5 arcsec/cy within Newtonian theory of gravitation have been considered:

- a) the perturbations of an intramercurial planet, Vulcan;

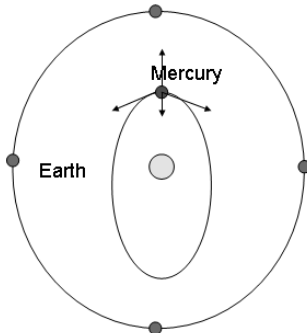


Fig. 6. – Stability of resonance between Mercury and Earth's orbits. Vectors representing gravitational forces acting upon Mercury, and Earth, are drawn at intervals of one orbit of Mercury.

b) the effects of a small quadrupole moment of the Sun, yielding a rosette-like orbit with advancing perihelion.

From an observative point of view: better observations of Mercury can be obtained when it is at the western or eastern elongation from the Sun, but in this case the motion of the planet is along the line of sight, and there are great errors on orbital elements estimation.

Valuable observations are made during transits (last one on May, 7 2003) when the motion is perpendicular to the line of sight. Observations from 1765 to now yield an anomalous precession of 43.1 ± 0.1 arcsec/cy explained by General Relativity as shown in table III [5].

Einstein equations fully explain the anomalous precession of the perihelion of Mercury

TABLE I. – *Planetary perturbations for Mercury.* [5]

Perturbator	Perturbation [arcsec/cy]	errorbar [arcsec/cy]
Venus	227.856	0.27
Earth	90.038	0.08
Mars	2.5536	0.00
Jupiter	153.584	0.00
Saturn	7.302	0.01
Uranus	0.141	0.00
Neptune	0.042	0.00
Solar Oblateness	0.010	0.02
Total Newtonian	574.069	0.30

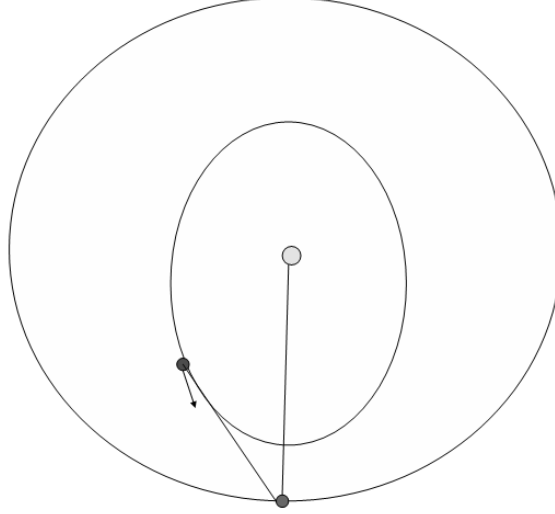


Fig. 7. – Measurement of orbital elements for Mercury: observative constraints. Mercury is better visible at its maximal elongations, but its velocity v at that time is almost always along the line of sight. Transits across the solar disk provide better conditions for v measurement.

[9] and of the other planets.

$$\delta\theta = 6\pi \cdot GM_{\odot}a/c^2b^2$$

with a, b semiaxes of ellipse $b = a \cdot (1 - e^2)^{1/2}$, e = eccentricity of the orbit.

Observations confirm Einstein predictions for the advancements of planetary perihelia. Since $\delta\theta \propto M_{\odot}/r$, with r orbital distance, this effect rapidly vanishes for planets far from the Sun. Note that for orbits around Earth,

$$\delta\theta_{\oplus}/\delta\theta_{\odot} = (M_{\oplus}/M_{\odot}) \cdot r_{\odot}/r_{\oplus} \sim 1/33 \text{ of the Mercury's value, for the}$$

closest orbit around Earth. Here $r_{\oplus} = 6578\text{km}$ i.e. 200 km above Earth surface, while $r_{\odot} = 50 \cdot 10^6$ km is the orbital radius of Mercury. For this reason the Moon shows a relativistic precession 1/2200 smaller than Mercury.

TABLE II. – General relativistic perturbations for Mercury. Third column shows the relative observability $e \cdot \delta\theta$: it is a parameter indicating that the more the orbit is elliptic the more is detectable the perihelion advancement [5].

Planet	Perturbation [arcsec/cy]	$e \cdot \delta\theta$ [arcsec/cy]
Mercury	43.03	8.847
Venus	8.63	0.059
Earth	3.84	0.064
Mars	1.35	0.126
Jupiter	0.06	0.003

TABLE III. – *Relativistic perturbations: comparison with observations.* [5]

Planet	Perturbation [arcsec/cy]	Observations [arcsec/cy]
Mercury	43.03	43.1 ± 0.1
Venus	8.63	8.65
Earth	3.84	3.85 or 4.6 ± 2.7 [5]
Mars	1.35	1.36
Moon	0.02	-

3. – Solar oblateness

There is a Newtonian precession in a quadrupole potential. Equation of quadrupole precession: $\Omega_q = -3/2\bar{\omega}_0 \cdot (R/r)^2 \cdot \cos(i)/(1 - e^2)^2 \cdot J_2$, where $J_2 = -Q_{33}/2MR^3$ is an adimensional parameter for quadrupole moment, R the solar radius and r is the orbital semiaxis, $\bar{\omega}_0$ the mean motion and i the inclination of the orbit with respect to the equatorial plane [10]. If $J_2 = 10^{-7}$ for the Sun (as from mass, rotation period and solar radius), the contribution to the precession experienced by Mercury should be 0.02 arcsec/cy. See table IV for comparison with Earth's case.

3.1. Solar disk astrometry. – Several Earthbased experiments have been conducted to measure the solar disk ellipticity. Main astrometric problems from the Earth are:

1) Astronomical refraction which is responsible of a non circular shape of the Sun, especially near the horizon. It was discovered by Tycho Brahe studying the Supernova of 1571. For moderate zenithal distances z , the increasement of height $\delta\Theta$ above the horizon of a point of the solar disk is

$$\delta\Theta \sim 60'' \cdot \tan(z).$$

The value of $\delta\Theta$ approaches the limit of $\delta\Theta \approx 34$ arcminutes near horizon. The previous formula no longer applies and Garstand's fit for airmass versus z is to be used [11]. Since the sun is still visible when its true upper limb is 34 arcminutes below the horizon the duration of the day is longer than that one calculated without astronomical refraction [12]. At horizon the figure of the Sun appears elliptical with vertical semiaxis smaller than the horizontal one up to 6 arcminutes (apparent oblateness).

2) Light aberration, which produces an effect along the solar equator, due to the rotation of the Sun around its axis.

3) Horizontal deformation, due to Earth's rotation. This is another aberration effect due to the Galilean composition of Earth's rotation velocity with respect to the Sun $v_{\odot} = v \cdot \cos(\lambda) \cdot \cos(a)$ and the speed of light c , with $v = 0.46$ km/s, λ the latitude, a the azimuth ($a=0$ when the Sun transits on the local meridian).

TABLE IV. – *Precession due to Solar oblateness ($J_2 = 10^{-7}$) and to Earth's one $J_{\oplus} \sim 1.083 \cdot 10^{-3}$*

Planet	Expected precession [arcsec/cy]
Mercury	0.02
Earth Oblateness	Around Earth satellite orbits are subjected to the quadrupole precession $d\vec{\Omega}_q/dt \propto -3/2\bar{\omega}_0 [R_{\oplus}/a/(1 - e^2)]^2 \cdot J_{2\oplus} \cdot \cos(i) \cdot \hat{\mathbf{n}}_{\oplus}$ i, inclination of the orbit, $\bar{\omega}_0$ satellite mean motion, a radius of the orbit.

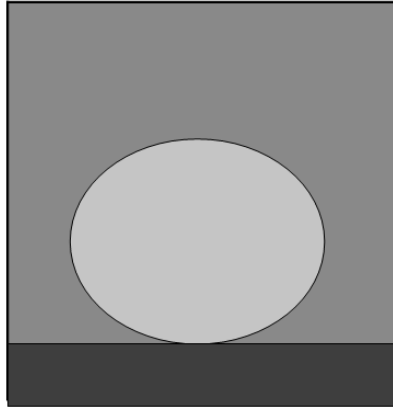


Fig. 8. – Solar disk apparent oblateness at sunset or sunrise.

The effect is slightly different from eastern to western solar limb because they are at different azimuth a , and it produces a small deformation on the horizontal direction.

3.2. Solar Disk Sextant. – It is the most recent experiment on the measurement of the Sun [13]. A rotating telescope above the atmosphere takes the positions of 10 points of the solar disk. Large photon statistics allow the precise location of those points. After data reduction for aberration and optical distortions the expected errorbar on the solar diameter is few milliarcseconds. the goal of this experiment is to detect secular variations of the solar diameter, beyond the 11-year sunspots' cycle.

4. – Relativistic light deflection

John Michell (1784) considering light as corpuscular, conceived the idea of a gravitating light and therefore of a black hole [14].

In general relativity $\Delta E = +0''.0047 \cdot 1/\tan(E/2)$ where E is the elongation of the star from the center of the Sun ($\Delta\Theta = 4GM_{\odot}/bc^2$). Remarkable is the effect done by Sun on the light coming from *Iades* cluster in occasion of the total solar eclipse of 1919 [15]. The Earth yields a similar $\Delta\Theta_{\oplus} = (10^6/12 \cdot 10^5) \cdot \Delta\Theta_{\odot}$, for an electromagnetic signal coming from a satellite orbiting at 600 km of altitude.

5. – Geodetic (de Sitter) Precession

Parallel transport (of a constant spin vector) in curved spacetime along a geodetic line (an orbiting body is actually in free fall, therefore along a geodetic line) generates a precession with respect to a fixed reference frame.

$$\vec{\Omega}_{dS} = 3/2 \cdot GM_{\odot}/c^2 r_{\odot}^3 \cdot (\vec{r} \wedge \vec{v}).$$

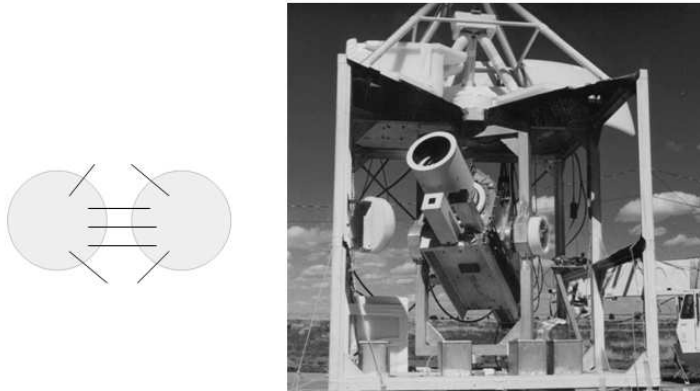


Fig. 9. – Solar Disk Sextant's focal plane CCD configuration. SDS is a Yale-NASA project to which the author has participated.

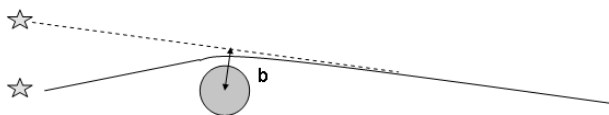


Fig. 10. – Relativistic light deflection by the solar mass.

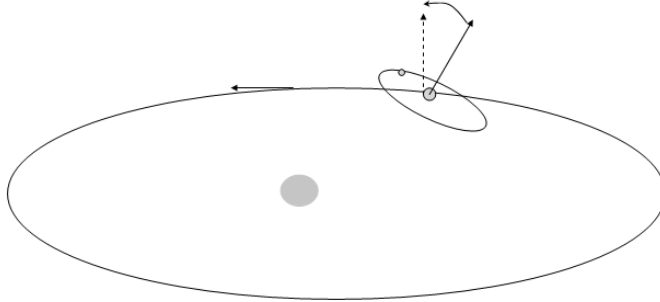


Fig. 11. – Scheme of de Sitter precession in the case of Moon’s orbital spin around the Sun.

This precession has been predicted by Wilhelm de Sitter [16]. For a spinning satellite at 600 km of altitude around Earth, after one orbit, such a precession is (for a circular orbit after applying third Kepler law) $\Theta_{dS} = 3/2GM_{\oplus}/c^2r^2 \cdot (vGM_{\oplus}/r_{\oplus})^{1/2} \sim 6.6$ arcsecs.

De Sitter precession depends on parallel transport in curved spacetime along geodesics, while Thomas precession occurs in flat spacetime (special relativity) with accelerated bodies (non geodesic motion). Thomas precession in General Relativity occurs when additional non gravitational strengths deviate the body from geodesic motion [17].

5.1. de Sitter precession of the Moon’s orbit. – After one Earth’s orbit such a precession is (again calculated for a circular orbit) $\Theta_{dS} = 3/2GM_{\odot}/c^2r^2 \cdot (vGM_{\odot}/r_{\odot})^{1/2} \sim 0.0192$ arcsecs. This precession has been measured within 2% of accuracy by Bertotti et al. (1987)[18]. Note that this precession is along the direction of the motion. After one orbit the ”spin vector” (in this case the orbital angular momentum of the Moon around Earth) precesses in the direction of the orbital motion.

5.2. Relativistic precessions as coupling between angular momenta. – Rewriting de Sitter precession formula as coupling between spin and orbital angular momenta

$$d\vec{S}/dt = 3/2 \cdot GM/mc^2r^3 \cdot (\vec{L} \wedge \vec{S})$$

where, in the previous case, \vec{S} is the orbital momentum of the Moon, or a constant spinning vector, and \vec{L} is the orbital momentum of the Earth-Moon system, or -in general- that one of the body carrying the constant spinning vector.

6. – Lense-Thirring precession

A constant spin vector orbiting around a spinning body, since rotational energy modifies spacetime, is subjected also to a relativistic spin-orbit coupling, which drags the

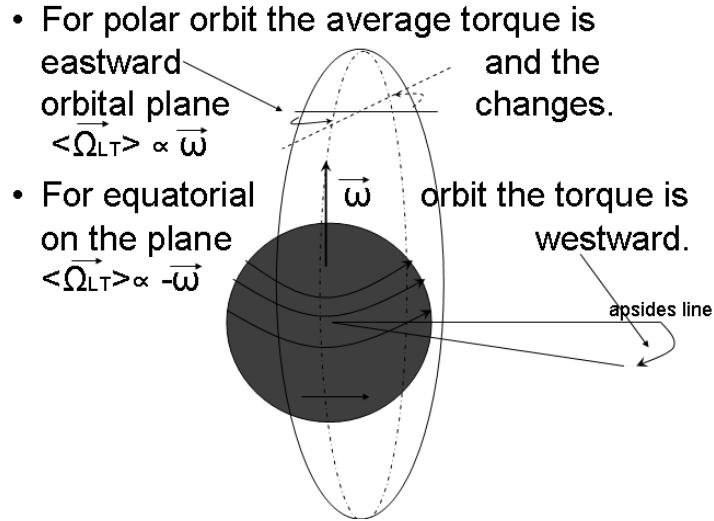


Fig. 12. – Lens-Thirring precession: scheme of the direction of the relativistic torque.

orbiting body out of the original orbital plane. The angular velocity vector of Lense-Thirring precession is

$\vec{\Omega}_{LT} = GI_{\oplus}/2c^2/R_{\oplus}^3 \cdot [3\vec{R}/R_{\oplus}^2 (\vec{\omega} \cdot \vec{R}) - \vec{\omega}]$, here R_{\oplus} is the Earth's radius, and \vec{R} is the position (vector) of the orbiting gyroscope; I and $\vec{\omega}$ the moment of inertia and angular velocity vector of the Earth [see Lense-Thirring papers reproduced in [4]] .

6.1. Lense-Thirring vs perihelion precession. – In 1917-18 Hans Thirring asked the astronomer Josef Lense to help him in calculating the effects of gravitational field around a rotating mass. For Mercury they found a precession 0.01 arcsecs/cy in the direction opposite to the rotation of the Sun, or to the orbital motion. For a polar orbit the precession (of apsidal line) occurs in the same direction of the rotation of the central mass, and a consequence of that is the changement of the original orbital plane (see figure 12). This effect is a consequence of general relativistic equation of motion and off-diagonal space-time components of the metric tensor which cannot be inferred by equivalence principle [17]. General Relativity predicts conditions under which the first Kepler Law, of planar and elliptic motion for two-body gravitational interaction, is no longer valid.

6.2. Lense-Thirring torques. – For an eastward rotating central mass, a body in polar orbit is subjected to an average torque eastward, and its orbital plane changes. $\langle \vec{\Omega}_{LT} \rangle \propto \langle \vec{\omega} \rangle$ (here $\langle \vec{\Omega} \rangle$ and $\langle \vec{\omega} \rangle$ are both average vectors). For an equatorial orbit the torque is on the plane and westward and $\langle \vec{\Omega}_{LT} \rangle \propto -\langle \vec{\omega} \rangle$.

$d\vec{L}/dt = (\vec{\Omega} \wedge \vec{L})$ rules the evolution of orbital angular momentum \vec{L} , precessing around the vector $\vec{\Omega}_{LT}$, Newtonian plane orbits (first Kepler's law) are changed into precessing *spherical orbits*.

If we think to the rotating central body as "dragging" the metric with it, and we test

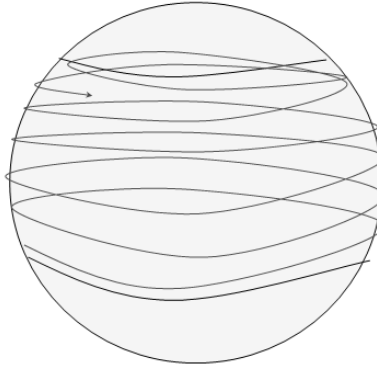


Fig. 13. – Sketch of a spherical orbit around a Kerr field. The body arises to a maximum latitude and turn back to a minimum one and so on.

the metric with an orbiting and spinning gyroscope, near the poles there is a tendency for the metric to rotate with the central body. Therefore a spin which is orbiting around that body precess in the direction of the rotating body. While near the equator the gravitational field and also the "dragging" of the metric falls off with increasing radial distance. If, then, we imagine the gyroscope, oriented so that its axis is perpendicular to that of the central rotating body, the side of the gyroscope nearest that body is dragged with the body more than the side away from it, so that the spin precesses in the opposite direction to the rotation of the body.

6.3. Lense-Thirring orbits in Kerr field. – The solution of Lense and Thirring are perturbative solutions, valid at first order in case of large distances and low $\vec{\omega}$ of central rotating body. More complicate orbits arise from positions near the horizon of a black hole or a neutron star, with whatever starting orbit. There are spherical belts of allowance within which the orbits occur. Those belts are drawn by precessing lines of apsides. (Wilkins, 1972)

6.4. Higher order torques. – In the Lense-Thirring effect the spin of the central mass drags the orbital angular momentum \vec{L} . If we consider the spin \vec{s} of the orbiting gyroscope, it is also subjected to a smaller torque $\propto (s/L) \cdot \Omega_{LT}$. Also de Sitter term appears $\propto (s/L) \cdot \Omega_{dS}$

7. – Pugh-Schiff precession

Instead of considering the precession of the lines of apsides of the elliptical orbit, the precession of the spinning axis of a torque-free gyroscope orbiting around Earth is studied for evidencing Lense-Thirring torques [17]. [Pugh's paper of 1959 has been reprinted in

TABLE V. – *Lense-Thirring timing corrections for planets' satellites ephemerides [see Lense-Thirring papers in [4]]*

Satellite	ΔT [s] after 100 years
Moon	13.9
Phobos (Mars)	0.5
Io (Jupiter)	29.5
Amalthea (Jupiter)	65.4
Mimas (Saturn)	19.2
Ariel (Uranus)	3.7

[4]). Such a study has started the project for the Gravity Probe-B satellite which is scheduled for launch in 2004 [19].

8. – The guide star for GP-B

Originally [20] Rigel, a 0.7 magnitude star laying near the celestial equator, was chosen as reference star for GP-B satellite. Afterwards IM Peg (*HR 8703*) of magnitude $M = 5.9$ has been selected[21]. It is a radio active star, close to a radio quasar. This has been done in order to measure very accurately its proper motion with VLBI, within 0.09 milliarcseconds of accuracy.

A beam splitter produces two images of the reference star for each readout axis subjected to photon counting statistical errors. Orbital light aberration (± 5 arcsecs and 90 minutes of period); annual aberration (± 20.116 arcsecs) and light deflections for Sun and planets produce large, very accurately known, periodic displacements. Those displacements appear in the readout of each gyroscope of GP-B, allowing a continuous calibration of the gyro scale of few parts in 10^7 , and a precision of 0.1 milliarcsecond over 3 years of experiment [see Everitt's paper in [4]].

REFERENCES

- [1] BARBIERI C., *Lezioni di Astronomia*, (Zanichelli, Bologna) 1999.
- [2] HOSKIN M., *Storia dell' Astronomia di Cambridge*, (Rizzoli, Milano) 2001.
- [3] AIRY G. B., *Proc. R. Soc. Lon.*, **20** (1871-2) 35.
- [4] RUFFINI R. SIGISMONDI C., *Nonlinear Gravitodynamics*, (World Scientific Pub. Singapore) 2003.
- [5] SCIAMA D.W., *La Relatività Generale*, (Zanichelli, Bologna) 1972.
- [6] FLAMMARION C., *Astronomie Populaire*, (G. Marpon et E. Flammarion, Éditeurs, Paris) 1880.
- [7] NEWCOMB S., *Astron. J.*, **14** (1894) 117.
- [8] MOYER A.E., *Simon Newcomb at the Nautical Almanac Office*, in *Proc. Nautical Almanac Office Sesquicentennial Symposium* (U.S. Naval Observatory, Washington D.C.) p. 129-146, 1999.
- [9] EINSTEIN A., *Preuss. Akad. Wiss. Berlin*, **47** (1915) 831.
- [10] CIUFOLINI I., *Physical Review Letters*, **56** (1986) 278.
- [11] GARSTANG R. H., *The Observatory*, **104** (1984) 196.
- [12] DUFFETT-SMITH P., *Astronomia Pratica*, (Sansoni, Firenze) 1983.
- [13] SOFIA S., ET AL., *Applied Optics*, **23** (1984) 1235.

- [14] MICHELL J., *Phil. Trans. R. Soc. Lon.*, **74** (1784) 35
- [15] EDDINGTON A. S., *The Observatory*, **42** (1919) 119.
- [16] DE SITTER W., *Mon. Not. R. Astron. Soc.*, **76** (1916) 199.
- [17] SCHIFF L. I., *Proc. Nat. Acad. Sci. Am.*, **46** (1960) 871.
- [18] BERTOTTI B., *Physical Review Letters*, **58** (1987) 1062.
- [19] GRAVITY PROBE-B WEBSITE, <http://einstein.stanford.edu/> (2004).
- [20] EVERITT C. W. F., *Proc. Int. School of Phys. Enrico Fermi Course LVI* Edited by B. Bertotti, NY-London Academic Press, 331, 1974.
- [21] RANSOM, R. R., ET AL., *Am. Astron. Soc. Meeting*, **194** (1999) 50.06.